



PII S0016-7037(97)00072-0

## No liquid immiscibility in the system MgSiO<sub>3</sub>-SiO<sub>2</sub> at 5.0 GPa

JOHN A. DALTON and DEAN C. PRESNALL

Magmalogy Laboratory, Department of Geosciences, University of Texas at Dallas, Richardson, Texas 75083-0688, USA

(Received October 9, 1996; accepted in revised form February 4, 1997)

**Abstract**—Liquidus phase relationships in the system MgSiO<sub>3</sub>-SiO<sub>2</sub> at 5.0 GPa have been determined using a multianvil apparatus. Compared to phase relationships at 1 atm, the MgSiO<sub>3</sub>-SiO<sub>2</sub> phase diagram at 5.0 GPa is significantly different in two respects. First, the composition of the eutectic between MgSiO<sub>3</sub> and SiO<sub>2</sub> moves from 65.0 wt% SiO<sub>2</sub> at 1 atm/1547°C (protoenstatite-cristobalite eutectic; Bowen and Andersen, 1914) to 68.8 wt% SiO<sub>2</sub> (orthoensatite-coesite eutectic) at 5.0 GPa/1930°C. Second, no stable two-liquid field is present in the MgSiO<sub>3</sub>-SiO<sub>2</sub> system at 5.0 GPa. The unbroken coesite liquidus curve is inflected indicating the presence of a submerged, metastable miscibility gap below the liquidus. Thus, although the temperature of the solvus critical point is likely to increase with pressure, the  $dT/dP$  slope of the SiO<sub>2</sub> liquidus is much steeper and as a result, the immiscibility dome has become submerged completely. The reduction in liquid immiscibility in the MgSiO<sub>3</sub>-SiO<sub>2</sub> system at 5.0 GPa implies that in more complex systems relevant to the Earth, immiscibility will also be suppressed at high pressures. Copyright © 1997 Elsevier Science Ltd

### 1. INTRODUCTION

The role of liquid immiscibility in igneous processes has long been debated (e.g., Roedder, 1979). At low pressures immiscibility may be a viable mechanism of differentiation during the late stages of fractionation of tholeiitic and possibly calc-alkaline magmas (Philpotts, 1982), while at higher pressures the possibility that liquid immiscibility may have been important in crust formation in the early Earth and Moon has been discussed (Massion and Koster van Groos, 1973; Hess et al., 1975). This latter hypothesis is particularly relevant in light of recent suggestions that two-liquid fields may be encountered in peridotitic melts at superliquidus temperatures (Navrotsky, 1992; Hess, 1996). The purpose of this investigation is to determine the MgSiO<sub>3</sub>-SiO<sub>2</sub> eutectic and extent of the two-liquid field in this system at 5.0 GPa. These data provide a preliminary foundation for study of immiscibility relationships in more complex systems relevant to cooling of an initially molten Earth.

### 2. PREVIOUS STUDIES

The MgO-SiO<sub>2</sub> system was first determined at 1 atm by Bowen and Andersen (1914), who located the eutectic between enstatite (MgSiO<sub>3</sub>) and cristobalite (SiO<sub>2</sub>) at 65 wt% SiO<sub>2</sub> and 1543°C, which is 1547°C (all subsequent temperatures are referred to ITS-90) when converted to the International Temperature Scale of 1990 (ITS-90, Preston-Thomas, 1990). Greig (1927) later determined the compositional limits of immiscibility at the liquidus in the silica-rich portion of this system to be 69 and 99 wt% SiO<sub>2</sub> at 1707°C, slightly below the melting point of cristobalite at 1723°C. This was confirmed by Ol'shanskii (1951) who found that the two-liquid field extends from 69 to 99.3 wt% SiO<sub>2</sub> at 1707°C. More recently, Hageman and Oonk (1986) investigated the entire region of immiscibility and showed that the two-liquid field is slightly skewed towards SiO<sub>2</sub> with a critical tempera-

ture of 1967°C at 88.9 wt% SiO<sub>2</sub>. In Fig. 1 we show the join MgSiO<sub>3</sub>-SiO<sub>2</sub> at 1 atm compiled from the above studies and Chen and Presnall (1975).

There has been little work on the effect of pressure on the MgSiO<sub>3</sub>-SiO<sub>2</sub> join. Chen and Presnall (1975) studied the Mg<sub>2</sub>SiO<sub>4</sub>-SiO<sub>2</sub> system at pressures from 1 atm to 2.5 GPa and showed that the composition of the enstatite-quartz eutectic does not measurably move from its 1 atm value. However, they did not determine the extent of the two-liquid field in this pressure range. In fact, there are few data on the effect of pressure on the two-liquid field in binary oxide systems, including MgSiO<sub>3</sub>-SiO<sub>2</sub>, although Circone and Agee (1995) have recently presented data on the TiO<sub>2</sub>-SiO<sub>2</sub> system at 3.0 GPa.

### 3. EXPERIMENTAL METHODS

#### 3.1. Starting Compositions

Five starting compositions with SiO<sub>2</sub> contents of 65 (MS-A), 85 (MS-B), 92 (MS-D), and 97 (MS-E) wt% were prepared from high purity oxides. Ten grams of each bulk composition were ground under methanol for 50 min and then fired for 2 h at temperatures ranging from 1550 to 1600°C. The resultant glass ( $\pm$  crystals) was then crushed and ground for a further 50 min. For the melting point determination of SiO<sub>2</sub>, we used amorphous silica of 99.999% purity (MS-C) obtained from Johnson Matthey (Alfa<sup>®</sup> Aesar<sup>®</sup> products). All starting compositions were stored in a vacuum desiccator prior to use.

#### 3.2. Experimental Technique

Approximately 1 mg of the required starting composition was loaded into 1.2 mm O.D. rhenium capsules. Rhenium was used as the capsule material in this study for it has been shown by previous workers (e.g., Presnall and Gasparik, 1990; Zhang et al., 1993; Presnall et al., 1997) to be a highly reliable capsule material at extreme temperatures in multianvil apparatus. The open capsule plus starting composition was dried at 1000°C for 1 h, closed by folding the open end and pressed to the required length of 2 mm.

All experiments were performed in a multianvil apparatus at the University of Texas at Dallas. Experiments were conducted with 18 mm octahedrons (95% MgO, 5% Cr<sub>2</sub>O<sub>3</sub>), WC cubes with 11 mm

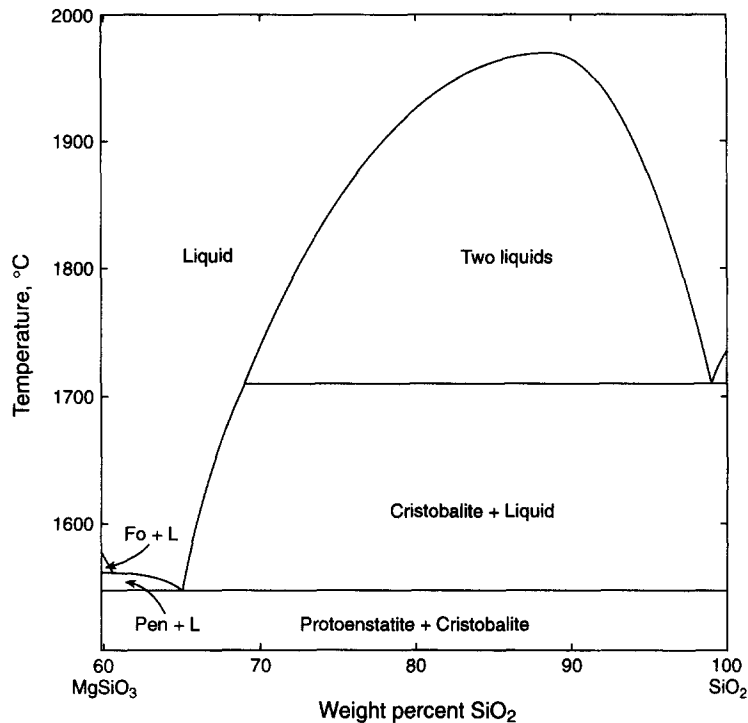


Fig. 1. The system  $\text{MgSiO}_3\text{-SiO}_2$  at 1 atm; compiled from Bowen and Andersen (1914), Greig (1927), Ol'shanskii (1951), Chen and Presnall (1975), and Hageman and Oonk (1986). Fo, forsterite; Pen, protoenstatite.

truncations, stepped graphite furnaces, and MgO spacers and thermocouple sleeves. Pressure calibration of the 18 mm assembly at high temperature is based on the quartz-coesite (3.03 GPa at 1100°C; Bohlen and Boettcher, 1982) and garnet-perovskite in  $\text{CaGeO}_3$  (6.0 GPa at 1140°C; Susaki et al., 1985) phase transitions, and melting point determination of diopside at 2.56 GPa (1680°C; Boyd and England, 1963). The pressure calibration curve is linear in the pressure range 2.5–6.0 GPa (Fig. 2). Temperatures were measured with W5%Re/W26%Re thermocouples positioned along the axis of the

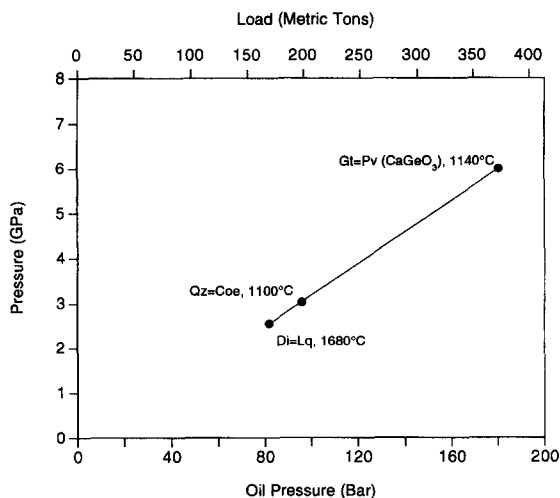


Fig. 2. Pressure calibration curve at high temperature for the 18 mm octahedron assembly. The quartz-coesite transition is from Bohlen and Boettcher (1982), the garnet-perovskite in  $\text{CaGeO}_3$  transition from Susaki et al. (1985) and the melting point of diopside from Boyd and England (1963).

graphite heater and in contact with the rhenium capsules. Because some of the temperatures required in this study exceed the calibrated range for this thermocouple (0–2300°C), we monitored temperature by directly recording the thermocouple EMF using the calibration of Asamoto and Novak (1967) with the corrections of Asamoto and Novak (1968). Although temperatures in some experiments were less than 2300°C, we chose to measure all temperatures in this manner in order to be internally consistent. At temperatures <2300°C, the EMF values determined by Asamoto and Novak (1967) are within  $\pm 4^\circ\text{C}$  of the manufacturer's EMF values for the particular batch of wire that we used. Temperatures were automatically controlled by a Eurotherm 818 solid state controller to within  $\pm 3^\circ\text{C}$  and were uncorrected for the effect of pressure on the EMF of the thermocouple. Prior to each experiment, the entire octahedron was dried for 30 min at 1000°C under nitrogen to remove any traces of water from the assembly. Load was applied until target pressure had been achieved, and then temperature was raised at a rate of 2.6 mV ( $\sim 180^\circ\text{C}$ ) per minute. The experimental conditions for each run are given in Table 1.

### 3.3. Duration of Experiments

It can be seen from Table 1 that run duration varies from 1 to 30 min. Ideally the length of a run should be sufficient to ensure equilibrium among the phases present. In the majority of experiments from previous multianvil studies at temperatures greater than 2000°C, quoted run durations are less than 5 min (e.g., Drake et al., 1993; Ito et al., 1995). Power fluctuations and thermocouple contamination are often given as reasons for such short run durations. In some cases, the thermocouple fails and temperature is estimated from power input. In the present study, we observed that at temperatures <2250°C, experiments could be performed for up to 30 min, after which they were quenched voluntarily. However, we experienced problems in maintaining run durations of greater than 10 min in experiments conducted at temperatures >2300°C. Experiments that successfully attained the required temperature usually followed the same pattern in power readings once the setpoint had been reached. That is, amps would fall, volts would remain the same or increase

Table 1. Run conditions and results.

Run	Starting composition	EMF (mV)	T (°C)	Time (minutes)	Result
MS4	MS-A	33.02	1950	30	Quench
MS5	MS-A	32.76	1930	30	Enstatite, Coesite, Quench
MS6	MS-A	32.50	1910	30	Enstatite, Coesite, Quench
MS14	MS-B	38.23	2450	15	Quench
MS15	MS-C	38.62	2500	5	Glass
MS19	MS-B	38.62	2500	6	Quench
MS20	MS-C	38.46	2480	5	Coesite + Glass
MS22	MS-B	34.88	2100	30	Coesite + Quench
MS23	MS-B	36.47	2250	30	Coesite + Quench
MS24	MS-B	37.41	2350	7	Coesite + Quench
MS25	MS-D	38.23	2450	7	Quench
MS27	MS-B	37.76	2390	1	Quench
MS28	MS-E	38.00	2420	15	Glass
MS29	MS-E	37.85	2400	8	Coesite + Quench

slightly, and the recorded temperature would deviate positively (up to 0.03 mV), but rarely negatively, from the setpoint. After a period of  $\geq 1$  min, the temperature would stop deviating in this manner, rise by approximately 1°C, hold for a few seconds, and then rise again. During this increase in temperature, the Eurotherm controller would be unable to bring the temperature back to the setpoint. If the run was not quenched immediately, temperature would continue to increase until the thermocouple became unstable. In an experiment quenched just after the mV increased in this manner from 38.62 (2500°C) to 38.9 (~2540°C) and became unstable, it was observed that the rhenium capsule partially melted, indicating temperatures in considerable excess of those recorded. This suggests that once the measured temperature begins to increase, the thermocouple reading is anomalous. Thus, through experience, we learned to quench the experiment the moment that this occurred.

Initially, we suspected that the reason behind the thermocouple problems was contamination of the thermocouple wires by material from some other part of the assemblage, e.g., MgO from the thermocouple sleeve. However, detailed microprobe examination of thermocouple wires revealed no detectable contaminant. Currently, we believe that oxidation of the thermocouple wires is responsible for the problems that we observe. It is known from piston-cylinder work that oxidation of tungsten-rhenium thermocouples is a problem at high temperatures and low pressures (e.g., Walter and Presnall, 1994). Our high temperature experiments at 5.0 GPa are at relatively low pressures for the multianvil device, and it is possible that we are encountering a similar problem, although further work is required to confirm this. All of the experiments at temperatures  $> 2300^\circ\text{C}$  given in Table 1 were quenched just as the temperature began to increase, and we believe that the temperatures given are correct. The consistency (see below) between these runs and those at lower temperature where oxidation was not a problem supports this conclusion.

### 3.4. Analytical Techniques

At the conclusion of each experiment the entire capsule was mounted longitudinally in epoxy resin and diamond polished for electron microprobe analysis. For experiments MS15 and MS20, the entire charge was removed from the capsule and mounted as a thin section for optical examination. The compositions of the solid and melt phases were determined by wavelength dispersive electron microprobe analysis using the JEOL JXA 8600 Superprobe at the University of Texas at Dallas. Crystalline phases were analyzed with a focused beam while a defocused beam of 15–20  $\mu\text{m}$  was used to analyze the melt phase. In both cases an acceleration voltage of 15 kV and a beam current of 10 nA were employed. Olivine (Mg) and quartz (Si) were used as the standards. Data were processed using the Bence-Albee matrix correction routine with the alpha coefficients of Albee and Ray (1970). To improve precision, multiple analyses of the melt phase were obtained.

## 4. RESULTS

### 4.1. General Observations

Figure 3 shows the phase diagram for MgSiO<sub>3</sub>-SiO<sub>2</sub> at 5.0 GPa constructed from the experiments tabulated in Table 1 and the liquid compositions given in Table 2. A temperature precision of  $\pm 20^\circ\text{C}$  has been placed on each experiment in accordance with our observations regarding the precision required to produce internally consistent data. The melting point of enstatite at 5.0 GPa is taken from Presnall and Gasparik (1990) and, following the work of Kanzaki (1990), we have taken coesite to be the stable polymorph of SiO<sub>2</sub> at 5.0 GPa, although we have not confirmed this. The melting point of SiO<sub>2</sub> at 5.0 GPa was determined from runs MS15 and MS20, which were examined optically under immersion oil where glass and crystals can be clearly distinguished. Our melting point determination of  $2480 \pm 20^\circ\text{C}$  compares well with the temperatures of  $2490^\circ\text{C}$  determined by Kanzaki (1990) and  $2500^\circ\text{C}$  by Zhang et al. (1993). The position of the eutectic at 5.0 GPa is located from runs MS4, 5, and 6 using starting composition MS-A (65 wt% SiO<sub>2</sub>). Both MS5 (1930°C) and MS6 (1910°C) contain the eutectic assemblage, enstatite, coesite, and liquid (Table 1). That both MS5 and MS6 contain all three phases is not surprising given that the temperatures of these two runs lie within experimental uncertainty. Orthoenstatite, the dominant phase in both of these runs, attains sizes of 100–150  $\mu\text{m}$ . Coesite, commonly  $< 10 \mu\text{m}$  in size, occurs in minor amounts but is slightly more abundant in MS6. The amount of quenched liquid in MS6 is very small and occurs only interstitially. In contrast, a large (~30% by volume) area of quenched liquid in MS5 is segregated toward the top of the charge and, for reasons discussed below, we use analyses of separated liquid from this run to obtain the eutectic composition (Table 2). From MS5 we obtain the eutectic composition 68.8 wt% SiO<sub>2</sub> at  $1930 \pm 20^\circ\text{C}$  (Fig. 3). Experiments MS22, 23, 24, and 29 all contain coesite plus quenched liquid (Table 1). In all cases, the coesite occurs as large (100–200  $\mu\text{m}$ ) sub-hedral crystals in the lower portion of the charge with the quench liquid occurring mainly at the top of the capsule but also interstitially between the crystals. The analyses presented in Table 2 are of the separated quench liquid.

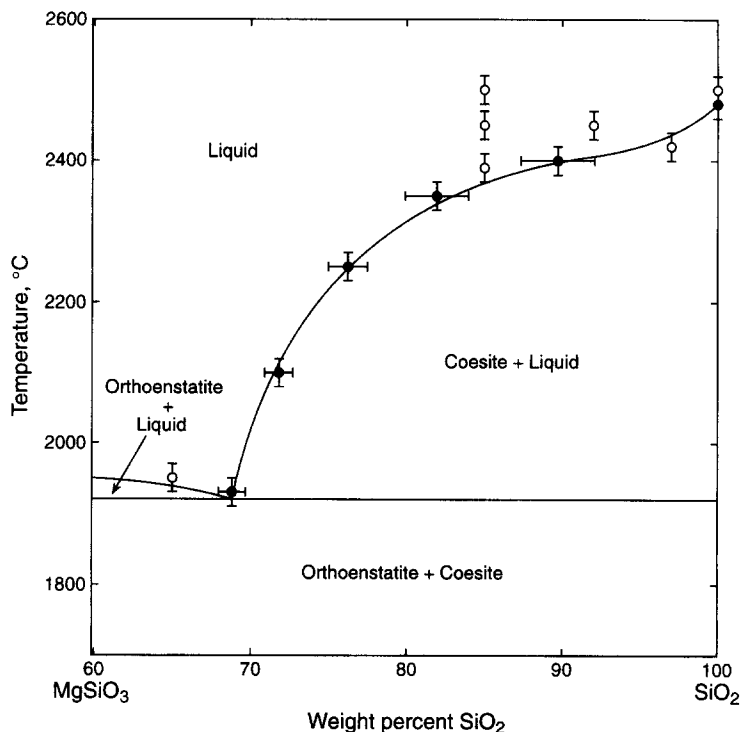


Fig. 3. The phase diagram for the  $\text{MgSiO}_3$ - $\text{SiO}_2$  system at 5.0 GPa. Open circles denote experiments in which liquid only was present and closed circles indicate liquid compositions from liquid + crystal experiments. All compositions have been normalized to a  $\text{MgO} + \text{SiO}_2$  sum of 100 wt%. Note the inflected shape of the coesite liquidus.

#### 4.2. Attainment of Equilibrium

The experiments could not be reversed because run times were restricted by thermocouple problems, as discussed in the preceding section. Consequently, equilibrium cannot be demonstrated, and the data that we report are synthesis results. It could, therefore, be argued that the short run durations at temperatures  $>2300^\circ\text{C}$  were of insufficient length to approach equilibrium. Two observations, however, suggests that this is not the case and a close approach to equilibrium was achieved.

First, the starting compositions used to define the coesite plus liquid field (MS-B and E) were all fired at 1 atm and temperatures ranging from  $1550$ – $1600^\circ\text{C}$ . From Fig. 1 this gives a starting composition which consists of cristobalite and a liquid of approximate composition 65–66 wt%  $\text{SiO}_2$ . During experiments at 5.0 GPa, this liquid should react with

coesite, and given sufficient time, would shift in composition to the equilibrium value for a given temperature. The length of run necessary to achieve this depends on temperature and liquid composition. The experiments given in Table 1 which define the coesite plus liquid field are all of differing length and temperature. Table 2 shows that for the runs in question (MS22, 23, 24, and 29), a marked change in liquid composition has occurred from that of the starting composition (65–66 wt%  $\text{SiO}_2$ ) to that quenched at  $P$  and  $T$ , indicating that equilibrium is being approached. Furthermore, there is good agreement between experiments run for 30 min (MS22 and 23) and those that were run for  $<10$  min (MS24 and 29) as can be seen on Fig. 3.

Second, detailed electron microprobe study of these runs show that the separated liquid is very homogenous but the interstitial liquid has been severely modified during quenching. In Fig. 4 we show three backscattered electron images

Table 2. Liquid compositions (wt%).

Run	Temperature ( $^\circ\text{C}$ )	Number of Analyses	$\text{SiO}_2$	$\text{MgO}$	Total
MS5	1930	20	69.00 (0.86) <sup>1</sup>	31.31 (0.94)	100.30
MS22	2100	31	71.65 (0.90)	28.15 (0.78)	99.80
MS23	2250	28	76.26 (1.25)	23.80 (1.11)	100.06
MS24	2350	22	82.78 (2.04)	18.26 (2.03)	101.04
MS29	2400	30	89.84 (2.37)	10.30 (2.09)	100.14

<sup>1</sup> Numbers in parentheses are two standard deviations.

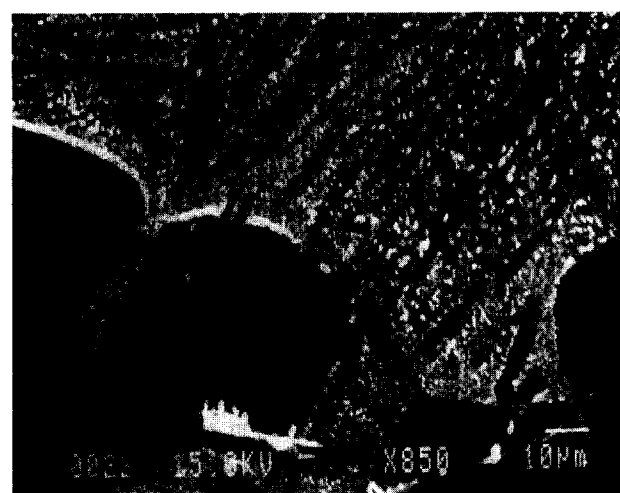
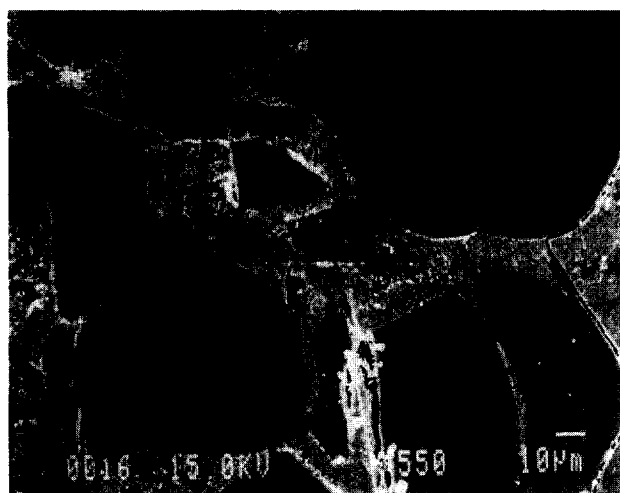


Fig. 4. Backscattered electron micrographs of experiment MS23 (2250°C). Beam conditions were 15 kV and 15 nA, and the scale bar in each case is 10  $\mu\text{m}$ . (a) Coesite crystals plus interstitial quench liquid in the lower portion of the charge. (b) Area of coesite plus interstitial quench liquid close to the left-hand wall of the capsule. (c) The boundary between the crystal + liquid and liquid-only areas of the charge.

(BEI) of experiment MS23 (2250°C). Figure 4a and 4b show interstitial quench liquid plus coesite while Fig. 4c shows the boundary between the separated quench liquid area and the crystals plus liquid area. The large coesite crystals in Fig. 4a display subhedral form but it can also be seen, particularly in the two large grains in the lower half of the image, that they have prominent teat-like features which have been produced on quench. Further quench textures can also be seen in Fig. 4b. Here we can see in the center right of the image, a  $\sim 10 \mu\text{m}$  diameter coesite grain growing out of the lower part of a much larger coesite grain (top right), and from the small grain one can see a quench coesite needle growing out from it. This is also evident in the center left of the image where a  $\sim 30 \mu\text{m}$  long coesite needle is attached to a coesite grain displaying prominent finger-like protrusions. A similar texture is shown in Fig. 4c, but this time quench needle-like coesite grains can be observed growing out of the stable coesite grain in the center of the image into the separated liquid area. Note also that the concentration of quench coesite is higher in the separated liquid region than in both the interstitial liquid region and the region directly adjacent to the top of the stable coesite grains where the separated liquid region begins. As the run is quenched isobarically through the solidus, the equilibrium coesite crystals form nuclei for growth of quench coesite, thus depleting the interstitial liquid in SiO<sub>2</sub>. Analysis of the interstitial liquid confirm this. Consequently, we present analyses of the separated liquid region which has not been quench-modified. The fact that such large quench modification can happen so rapidly on quench points to quite high reaction rates for this system at the temperatures of the experiments. This, together with the observed shift in the composition of the liquid from the starting material to that analyzed at the top of the capsule, indicates that, despite the short run times, our experiments approached equilibrium.

### 5. LIQUID IMMISCIBILITY AT 5.0 GPa

There was no evidence in any of our experiments to indicate the presence of a stable two-liquid field at 5.0 GPa. The inflected shape of the liquidus curve in Fig. 3 indicates the presence of a submerged, metastable miscibility gap below the liquidus as occurs in the system BaO-SiO<sub>2</sub> at 1 atm (Seward et al., 1968). It can be seen from Fig. 3 that at 5.0 GPa, the topology of the MgSiO<sub>3</sub>-SiO<sub>2</sub> phase diagram is

Table 3. A comparison of 1 atm vs. 5.0 GPa phase relations for MgSiO<sub>3</sub>-SiO<sub>2</sub>.

	1 atm	5.0 GPa
Solidus temperature	1547°C	1930°C
Eutectic liquid composition	65 wt% SiO <sub>2</sub>	68.8 wt% SiO <sub>2</sub>
Monotectic temperature	1707°C	—
Monotectic liquid compositions		
MgO-rich liquid	69 wt% SiO <sub>2</sub>	—
SiO <sub>2</sub> -rich liquid	99.3 wt% SiO <sub>2</sub>	—
Critical point	1967°C	—
Critical point composition	88.9 wt% SiO <sub>2</sub>	—
Melting point of SiO <sub>2</sub>	1723°C	2480°C
Melting point of MgSiO <sub>3</sub>	1557°C	1962°C

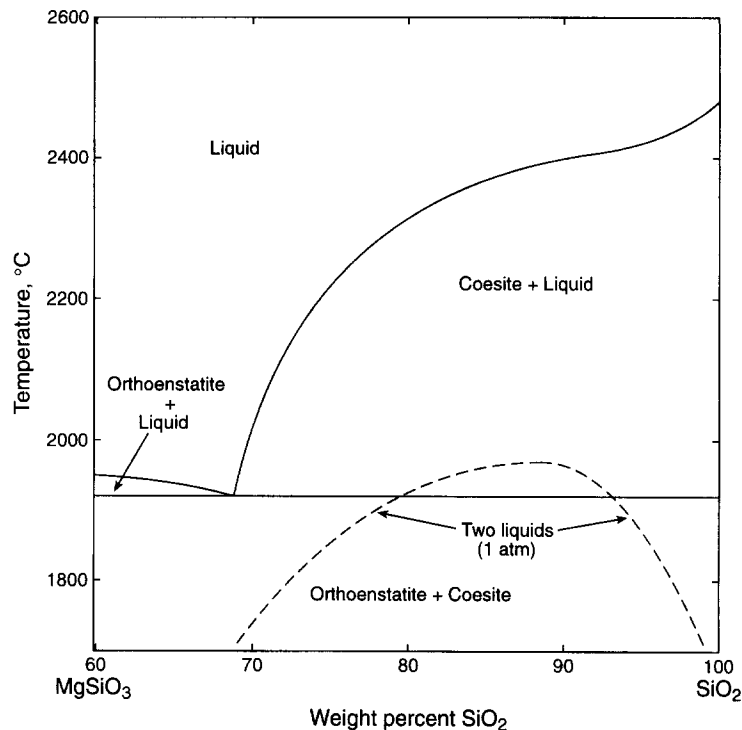


Fig. 5. The 1 atm solvus (dashed curve) compared to the phase diagram at 5.0 GPa.

very different from that at 1 atm (Fig. 1). The eutectic is shifted to a more  $\text{SiO}_2$ -rich composition from 1 atm and the stable two-liquid field has disappeared altogether (Fig. 3). Table 3 outlines the principal differences between the 1 atm and 5.0 GPa phase diagrams, and Fig. 5 compares the topology at 5.0 GPa as shown in Fig. 3 with the position of the solvus at 1 atm.

From Table 3 one can see that the melting point of  $\text{SiO}_2$  has increased substantially ( $757^\circ\text{C}$ ) from 1 atm to 5.0 GPa. Although the temperature of the critical point is likely to increase with pressure, our data indicate that the  $dT/dP$  slope of the  $\text{SiO}_2$ -liquidus is much steeper, which causes the former to become submerged below the latter. As a result, the immiscibility dome is buried beneath the liquidus in the subliquidus regime producing an inflected liquidus as we observe (Fig. 3).

**Acknowledgments**—We thank Kavin Morris for invaluable technical assistance and Y.-H. Weng for some of the runs used to define the pressure calibration curve. Dr. A. Navrotsky and two anonymous reviewers are thanked for their thorough reviews of the manuscript. This research was supported by Texas Advanced Research Program Grant No. 009741-044 and National Science Foundation grant EAR-9219159. Department of Geosciences, University of Texas at Dallas contribution number 852.

#### REFERENCES

- Albee A. L. and Ray L. (1970) Correction factors for electron-probe microanalysis of silicates, oxides, carbonates, and sulphates. *Anal. Chem.* **42**, 1408–1414.
- Asamoto R. R. and Novak P. E. (1967) Tungsten-Rhenium thermocouples for use at high temperature. *Rev. Sci. Instrum.* **38**, 1047–1052.
- Asamoto R. R. and Novak P. E. (1968) Erratum: Tungsten-Rhenium thermocouples for use at high temperature. *Rev. Sci. Instrum.* **39**, 1233.
- Bohlen S. R. and Boettcher A. L. (1982) The Quartz  $\rightleftharpoons$  Coesite transformation: A precise determination and the effects of other components. *J. Geophys. Res.* **87**, 7073–7078.
- Bowen N. L. and Andersen O. (1914) The binary system  $\text{MgO-SiO}_2$ . *Amer. J. Sci.* 4th ser. **37**, 487–500.
- Boyd F. R. and England J. L. (1963) Effect of pressure on the melting of diopside,  $\text{CaMgSi}_2\text{O}_6$ , and albite,  $\text{NaAlSi}_3\text{O}_8$ , in the range up to 50 kilobars. *J. Geophys. Res.* **68**, 311–323.
- Chen C.-H. and Presnall D. C. (1975) The system  $\text{Mg}_2\text{SiO}_4\text{-SiO}_2$  at pressures up to 25 kilobars. *Amer. Mineral.* **60**, 398–406.
- Circone S. and Agee C. B. (1995) Effect of pressure on cation partitioning between immiscible liquids in the system  $\text{TiO}_2\text{-SiO}_2$ . *Geochim. Cosmochim. Acta* **59**, 895–909.
- Drake M. J., McFarlane E. A., Gasparik T., and Rubie D. C. (1993) Mg-perovskite/silicate melt and majorite garnet/silicate melt partition coefficients in the system  $\text{CaO-MgO-SiO}_2$  at high temperatures and pressures. *J. Geophys. Res.* **98**, 5427–5431.
- Greig J. W. (1927) Immiscibility in silicate melts. *Amer. J. Sci.* **13**, 1–154.
- Hageman V. B. M. and Oonk H. A. J. (1986) Liquid immiscibility in the  $\text{SiO}_2 + \text{MgO}$ ,  $\text{SiO}_2 + \text{SrO}$ ,  $\text{SiO}_2 + \text{La}_2\text{O}_3$ , and  $\text{SiO}_2 + \text{Y}_2\text{O}_3$  systems. *Phys. Chem. Glasses* **27**, 194–198.
- Hess P. C. (1996) Upper and lower critical points: Thermodynamic constraints on the solution properties of silicate melts. *Geochim. Cosmochim. Acta* **60**, 2365–2377.
- Hess P. C., Rutherford M. J., Guillemette R. N., Ryerson F. J., and Tuchfield H. A. (1975) Residual products of fractional crystallization of lunar magmas: An experimental study. *Proc. 6th Lunar Sci. Conf.* **1**, 895–909.
- Ito E., Morooka K., Ujike O., and Katsura T. (1995) Reactions between molten iron and silicate melts at high pressure: Implications for the chemical evolution of the Earth's core. *J. Geophys. Res.* **100**, 5901–5910.
- Kanzaki M. (1990) Melting of silica up to 7 GPa. *J. Amer. Ceramic Soc.* **73**, 3706–3707.
- Massion P. J. and Koster van Groos A. F. (1973) Liquid immiscibility in silicates. *Nature Phys. Sci.* **245**, 60–63.

- Navrotsky A. (1992) Unmixing of hot inorganic melts. *Nature* **360**, 306.
- Ol'shanskii Ya. I. (1951) Equilibria of two immiscible liquids in systems of alkaline earth silicates. *Dokl. Akad. Nauk S.S.S.R.* **76**, 93–96.
- Philpotts A. R. (1982) Compositions of immiscible liquids in volcanic rocks. *Contrib. Mineral. Petrol.* **80**, 201–218.
- Presnall D. C. and Gasparik T. (1990) Melting of enstatite (MgSiO<sub>3</sub>) from 10 to 16.5 GPa and the forsterite (Mg<sub>2</sub>SiO<sub>4</sub>)—majorite (MgSiO<sub>3</sub>) eutectic at 16.5 GPa: Implications for the origin of the mantle. *J. Geophys. Res.* **95**, 15771–15777.
- Presnall D. C., Weng Y.-H., Milholland C. S., and Walter M. J. (1997) Liquidus phase relations in the system MgO-MgSiO<sub>3</sub> at pressures to 25 GPa—Constraints on crystallization of a molten Hadean mantle. *Phys. Earth Planet. Intl.* (in press).
- Preston-Thomas H. (1990) The International Temperature Scale of 1990 (ITS-90). *Metrologia* **27**, 3–10, 107.
- Roedder E. (1979) Silicate liquid immiscibility in magmas. In *The Evolution of The Igneous Rocks Fiftieth Anniversary Perspectives* (ed. H. S. Yoder), pp. 15–59. Princeton Univ. Press.
- Seward T. P., Uhlmann D. R., and Turnbull D. (1968) Phase separation in the system BaO-SiO<sub>2</sub>. *J. Amer. Ceram. Soc.* **51**, 278–285.
- Susaki J., Akaogi M., Akimoto S., and Shimomura O. (1985) Carnet-Perovskite transformation in CaGeO<sub>3</sub>: In situ X-ray measurements using synchrotron radiation. *Geophys. Res. Lett.* **12**, 729–732.
- Walter M. J. and Presnall D.C. (1994) Melting behavior of simplified lherzolite in the system CaO-MgO-Al<sub>2</sub>O<sub>3</sub>-SiO<sub>2</sub>-Na<sub>2</sub>O from 7 to 35 kbar. *J. Petrol.* **35**, 329–359.
- Zhang J., Liebermann R. C., Gasparik T., and Herzberg C. T. (1993) Melting and subsolidus phase relations of SiO<sub>2</sub> at 9–14 GPa. *J. Geophys. Res.* **98**, 19785–19793.